Available online at www.sciencedirect.com
SCIENCE DIRECT
Polymer 46 (2005) 11673–11689
polymer
www.elsevier.com/locate/polymer

TPO based nanocomposites. Part 1. Morphology and mechanical properties

Hyuk-soo Lee [a], Paula D. Fasulo [b], William R. Rodgers [b], D.R. Paul [a,*]

[a] Department of Chemical Engineering and Texas Materials Institute, The University of Texas at Austin, Austin, TX 78712, USA
[b] General Motors Research and Development Center, 30500 Mound Road, Warren, MI 48090, USA

Received 22 July 2005; received in revised form 12 September 2005; accepted 15 September 2005
Available online 14 October 2005

Abstract

The relationship between morphology and the mechanical properties of thermoplastic olefin (TPO) materials that are reinforced with organoclay fillers and prepared by melt processing is reported. Nanocomposites based on blends of polypropylene and elastomer and using an organoclay masterbatch were prepared in a twin-screw extruder. Transmission electron microscopy, atomic force microscopy and wide-angle X-ray scattering were employed to carry out a detailed particle analysis of the morphology of the dispersed clay and elastomer phases for these nanocomposites. The improvement in mechanical properties, e.g. stiffness enhancement as evaluated by stress–strain analysis and impact strength obtained from notched Izod impact tests, were successfully explained in terms of morphological changes induced by the presence of the clay and elastomer particles. Quantitative analyses of TEM micrographs and AFM images revealed a decrease in the aspect ratio of the clay particles and a reduction in the size of elastomer particles with increasing clay content. In addition, WAXD scans indicated a skin–core effect for the injection molded specimens in terms of both polypropylene crystal orientation and clay filler orientation. This information is essential for the understanding of the mechanism of mechanical property enhancement in nanocomposite materials.

Keywords: Polymer nanocomposites; Polypropylene; Elastomer

1. Introduction

The use of layered silicates as fillers in polymers has gained considerable attention due to the ability to achieve exceptional property enhancements at very low loading levels [1–4]. In recent years, a concerted effort has been made to disperse layered silicates in low cost polyolefins, like polypropylene (PP) [5–15]. PP has many desirable properties, such as low density, high thermal stability, and good solvent resistance; however, its modulus relative to engineering polymers, e.g. nylon 6, polycarbonate, etc. is low [16]. This issue is often addressed by adding conventional fillers, e.g. talc or glass fibers [17–19]. Unfortunately, due to the size (or aspect ratio) of such fillers, large loadings are required to significantly increase stiffness, which can result in poor processability, lower ductility, and a rough surface finish. Replacing such fillers with layered silicates could potentially alleviate these issues, assuming good levels of clay dispersion can be achieved. The data in Fig. 1 shows that addition of only 5 wt% montmorillonite (MMT) to a thermoplastic polyolefin (TPO) gives equivalent stiffness enhancement as 20 wt% talc; these data are typical of current commercial formulations [20].

Although complete exfoliation of clay particles in PP nanocomposites has not been reported to date, the stiffness improvement achieved at low clay loadings is attractive from an industrial point of view; however, addition of filler usually sacrifices the toughness of these materials particularly at low temperatures. The latter has been a major issue for some applications in which an optimum balance of stiffness and toughness is desired; to address this, an elastomer component has been incorporated into PP/filler composites, producing ternary-phase polymer composites [21–25]. Elastomer toughened PP or TPO materials containing talc as a filler are widely used to produce automotive exterior and interior parts; however, the use of large amounts of filler, e.g. >20 wt%, which is required to achieve desirable properties, results in some processing and performance compromises as described above. Also, it has been reported that the morphology of the dispersed phases plus elastomer and filler contents as well as processing conditions play an important role in determining the stiffness and toughening behavior of PP/elastomer/filler

* Corresponding author. Tel.: +1 512 471 5392; fax: +1 512 471 0542.
E-mail address: drp@che.utexas.edu (D.R. Paul).

0032-3861/$ - see front matter © 2005 Elsevier Ltd. All rights reserved.
doi:10.1016/j.polymer.2005.09.068

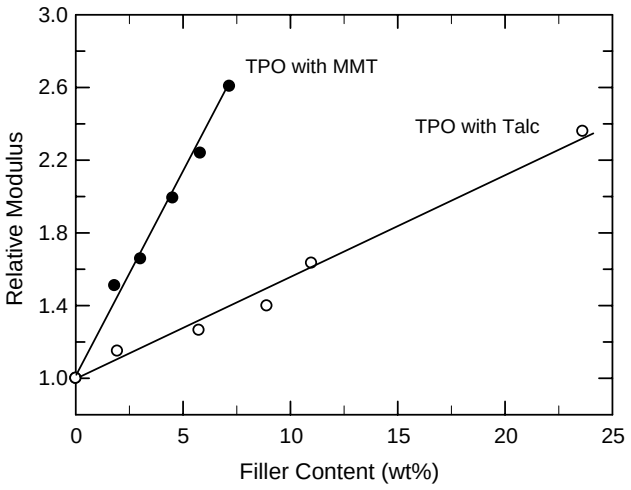

Fig. 1. Comparison of relative modulus as a function of filler content of TPO composites formed from melt mixing with MMT and with talc; data from Ref. [20].

composites [23,25,26]. To date, only a few studies have addressed the morphology and mechanical properties, e.g. tensile and impact properties, and their relationships for PP/elastomer/organoclay nanocomposites [19,27,28]; a systematic study of how morphology affects the mechanical properties of TPO nanocomposites has not been reported.

The purpose of this study is to examine the morphology and mechanical properties of PP reinforced with an organoclay and toughened with an ethylene–octene based elastomer made by melt processing. To promote exfoliation of clay platelets in PP, a polypropylene-*grafted*-maleic anhydride (PP-*g*-MA) material is premixed with the organoclay prior to melt processing. A detailed particle analysis for both filler and elastomer phases is presented and used to understand the mechanical properties of these nanocomposites. As expected, the mechanical properties of the injection-molded specimens depend strongly on the morphology of the dispersed clay and elastomer particles. Subsequent papers will discuss the thermal expansion behavior and the modeling of stiffness and thermal expansion of these nanocomposites.

2. Experimental

2.1. Materials and composite preparation

Nanocomposites were formed by melt compounding mixtures of PP (melt index = 37), an ethylene–octene based elastomer (melt index = 0.5) and a masterbatch material containing equal parts of maleated PP (PP-*g*-MA, MA content = 1.0 wt%) and an organically modified montmorillonite (di-methyl, dihydrogenated tallow- montmorillonite). Compounding was carried out using a Hakke co-rotating twin screw extruder (length = 305 mm, *L*/*D* = 10) set at a barrel temperature of 170 °C (feed), a die temperature of 190 °C, a screw speed of 280 rpm, and a feed rate of 1 kg/h.

Extruded nanocomposites pellets were dried and then formed into standard tensile (ASTM D638, Type I) and Izod (ASTM D256) bars in an Arburg Allrounder 305-210-700 injection molding machine using a barrel temperature of 190 °C (feed) to 220 °C (die), mold temperature of 40 °C, injection pressure of 35 bar, and a holding pressure of 35 bar. The amount of montmorillonite (MMT) in each extruded batch was determined by placing the central portion of a tensile bar or Izod bar in a furnace at 900 °C for 45 min and weighing the remaining MMT ash with appropriate correction for loss of structural water during incineration.

2.2. Morphology characterization and particle analysis for the filler and elastomer

Samples for TEM analysis were taken from the central and skin regions of an Izod bar. The central sample regions were located parallel and perpendicular to the flow direction ca. 3–4 cm away from the far end of a 13 cm Izod bar and half-way between the top and bottom surfaces of the bar. Sections taken from the core region of injection-molded specimens were viewed parallel to the three orthogonal axes, flow direction (FD), transverse direction (TD), and normal direction (ND). This nomenclature is used throughout the remainder of this paper. In what follows, transmission electron microscopy, TEM, analyses were made on a view observed parallel to the transverse direction, or TD (FD–ND plane), as shown in Fig. 2; the morphologies viewed parallel to the flow direction, or FD (TD–ND plane), and the normal direction, or ND (FD–TD plane), will be presented in subsequent papers. Ultra-thin sections ranging from 50 to 70 nm in thickness were cryogenically cut with a diamond knife at temperatures of −65 °C for the specimen and −58°C for the knife using a Reichert–Jung Ultracut E microtome. Sections were collected on 300 mesh copper TEM grids and subsequently dried with filter paper. The sections were examined by TEM using a JEOL 2010F TEM with a LaB_6 filament operating at an accelerating voltage of 120 kV.

TEM images, typically 30 K in magnification for standard negative film, were electronically scanned and converted into grayscale tagged-image file format (TIFF) image files. Quantitative image analysis was performed by opening a digital file in Adobe Photoshop where the dispersed platelets and/or agglomerates are traced over into an overlapped blank layer. To ensure accurate measurements of the particle length and thickness, the image is sufficiently magnified so that most of the particles, including single platelets, are counted. The resulting black/white layer file is imported into the image

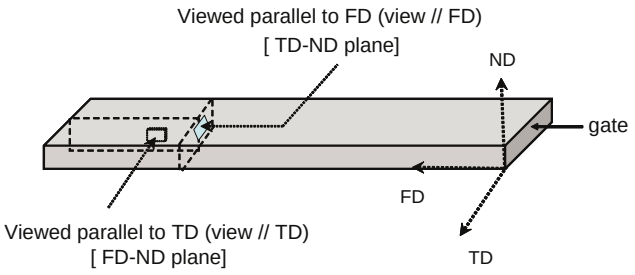

Fig. 2. Illustration of TEM sampling location in relation to flow (FD), transverse (TD), and normal directions (ND) of an injection-molded bar.

analysis program, SigmaScan Pro, which analyzes the traced particles, assigns each particle a numerical label, and exports the particle's length and thickness to separate files.

Atomic force microscopy (AFM) experiments were performed on cryogenically microtomed surfaces of nanocomposites containing elastomer using a Digital Instruments Dimension 3100 with Nanoscope IV controller at room temperature. Images were recorded in the tapping mode using etched silicon probes. The instrumental parameters such as the set point and the gains were adjusted to improve the image resolution.

WAXD was conducted using a Sintag XDS 2000 diffractomer in the reflection mode using an incident x-ray wavelength of 1.542 Å at a scan rate of 1.0 °/min in a range of $2\theta = 1$–$30°$. X-ray analyses were performed at room temperature on milled (e.g. top 1.6 mm removed from 3.2 mm thick Izod bars) and unmilled Izod bars to reveal the structure in the skin and in the core of the injection molded specimens, respectively. The Izod specimens were oriented such that the incident beam reflected off the transverse face.

2.3. Mechanical properties

Stress–strain analyses were performed according to ASTM D638 using an Instron model 1137 upgraded for computerized data acquisition. Modulus was determined using an extensometer at a crosshead speed of 0.51 cm/min, while yield strength and elongation values were determined at a speed of 0.51 cm/min for nanocomposites with no elastomer and at a speed of 5.1 cm/min for nanocomposites containing elastomer. Tensile property values reported here represent an average from measurements on at least five specimens. Flexural tests were performed according to ASTM D790 at a speed of 1.27 mm/min. Notched Izod impact tests were performed at room temperature using a TMI Izod tester (6.8 J hammer and 3.5 m/s impact velocity) according to ASTM D256. Property values reported here represent an average from, at least, five specimens.

3. Results and discussion

3.1. Morphology characterization using TEM and AFM

The aspect ratio of the clay particles, i.e. particle length/particle thickness, is one of the important factors in determining the reinforcement efficiency of clay nanocomposites and must be known quantitatively for modeling mechanical and thermal expansion behavior [29,30]. However, the details of the dimensions of the clay particles, i.e. the particle length and thickness, in nanocomposites has not typically been statistically quantified in most studies, especially for less exfoliated systems such as polyolefin and TPO nanocomposites. Recently, a few studies have addressed the issue of clay dimensions in polymer nanocomposites using AFM techniques [2,31,32]. Such techniques, however, may not be useful in polyolefin and TPO nanocomposites due to the surface roughness of specimens induced by the difference in thermal expansion between the clay and polyolefin matrix since specimens are typically cryogenically prepared with subsequent measurements at room temperature. This substantial difference in the temperature of sample preparation and measurement results in very rough surfaces. In order to address the issue of aspect ratios for these nanocomposites, a careful characterization of nanocomposite morphology using TEM and an extensive particle analysis is needed.

Fig. 3(a) shows a TEM micrograph of the PP-*g*-MA/organoclay masterbatch, containing ca. 30 wt% MMT, used in this work; this view is parallel to the TD (FD–ND plane) of an injection molded bar of this nanocomposite concentration. Most of the clay particles appear as an intercalated bundle with a preferred orientation; whereas, the clay particles observed parallel to the FD (TD–ND plane) are randomly oriented and have a shorter length and curved shape compared to those viewed parallel to the TD, see Fig. 3(b).

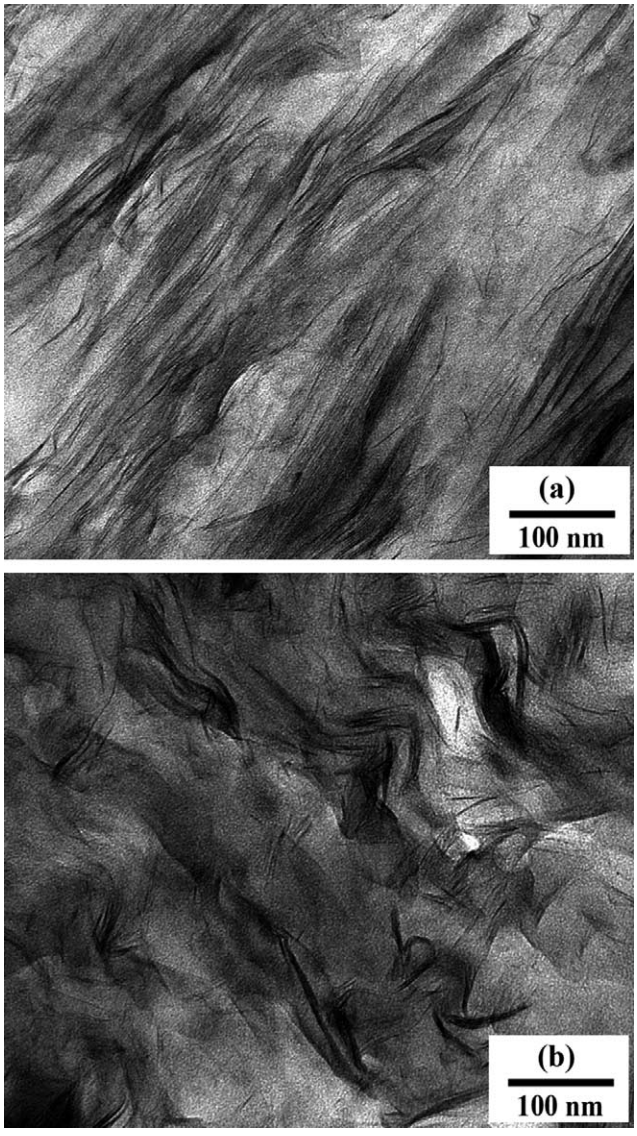

Fig. 3. TEM micrographs of the PP-*g*-MA/organoclay masterbatch: (a) viewed parallel to the TD and (b) viewed parallel to the FD.

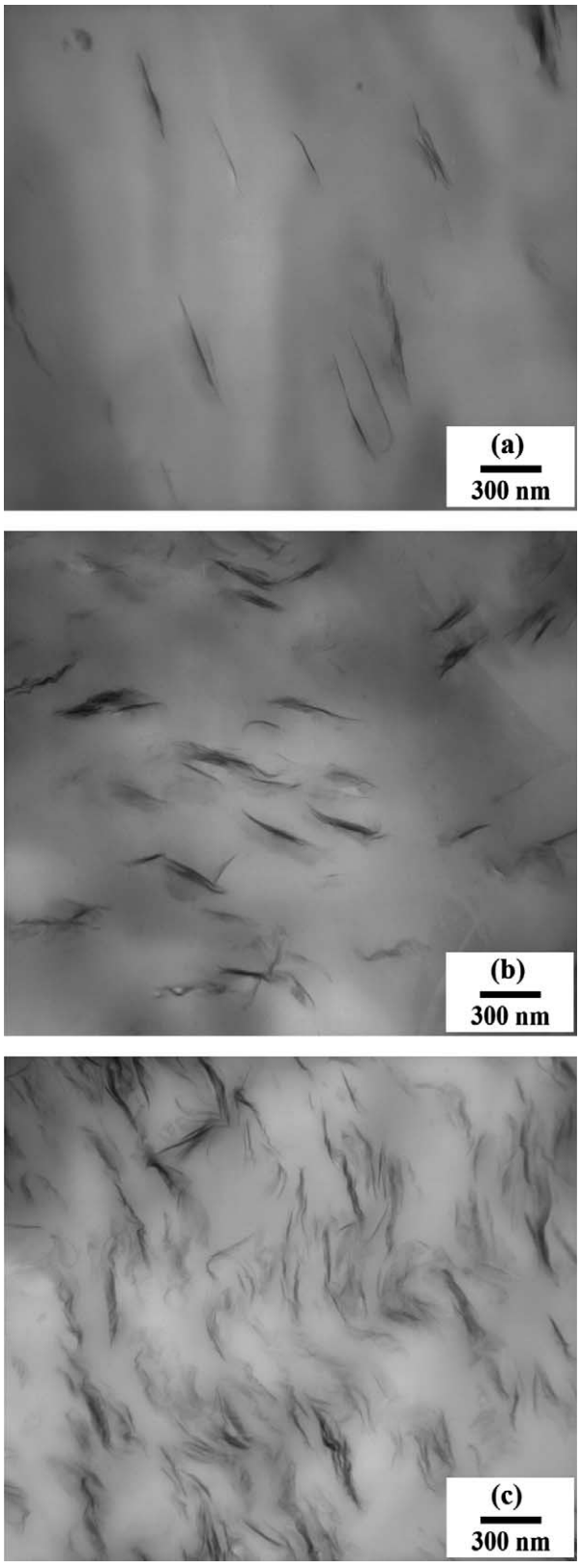

Fig. 4. TEM micrographs of PP/masterbatch nanocomposites containing (a) 1 wt%, (b) 2.8 wt% and (c) 6.8 wt% MMT. Images were taken from the core of injection molded specimens and viewed parallel to the TD.

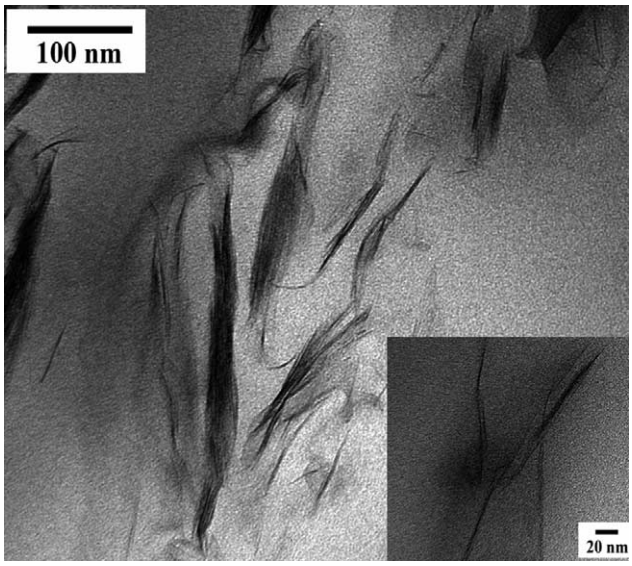

Fig. 5. Typical TEM micrograph of PP/masterbatch nanocomposites showing a mixed morphology consisting of intercalated clay tactoids and exfoliated clay platelets.

Fig. 4 shows TEM micrographs of PP/masterbatch nanocomposites containing 1, 2.8 and 6.8% by weight of MMT taken from the core and viewed parallel to the TD. As shown in these TEM micrographs and a typical TEM micrograph in Fig. 5, these nanocomposites have a mixed morphological structure, i.e. combination of intercalated stacks and exfoliated particles. Also, it is noted that a large portion of the clay particles appears as bent, skewed and/or curved structures when viewed parallel to the TD axis (FD–ND plane). However, it is also evident that the length and thickness of the clay particles vary with MMT concentration in the nanocomposites. To address this issue, quantitative TEM particle analysis was performed, and the results will be discussed in Section 3.2.

Recently, Mirabella et al. reported that addition of organoclay caused a reduction of rubber particle size in PP/elastomer blends [28]. They attributed the apparent reduction in rubber particle size to the increase in melt viscosity as clay loading increases and/or the role of clay as a chemical modifier for the rubber phase. In our TPO nanocomposite system, we may expect a similar reduction in elastomer particle size caused by higher forces induced by the higher melt viscosity as MMT content increases; this may explain, in part, some of the trends in impact properties and thermal expansion of the current nanocomposites to be discussed later in this and subsequent papers.

Fig. 6 shows TEM micrographs of PP/elastomer/masterbatch nanocomposites containing 30% elastomer and various amounts of MMT, which were viewed parallel to the TD. In TEM micrographs of PP/elastomer blends with no clay, rather elongated elastomer particles ranging in size from ca. 1 to 7 μm were observed, Fig. 6(a). The addition of 1 wt% MMT to the PP/elastomer blend leads to an apparent reduction in the size of the elastomer particles and a change in their shape as shown in Fig. 6(b). The elastomer particles are still much larger than

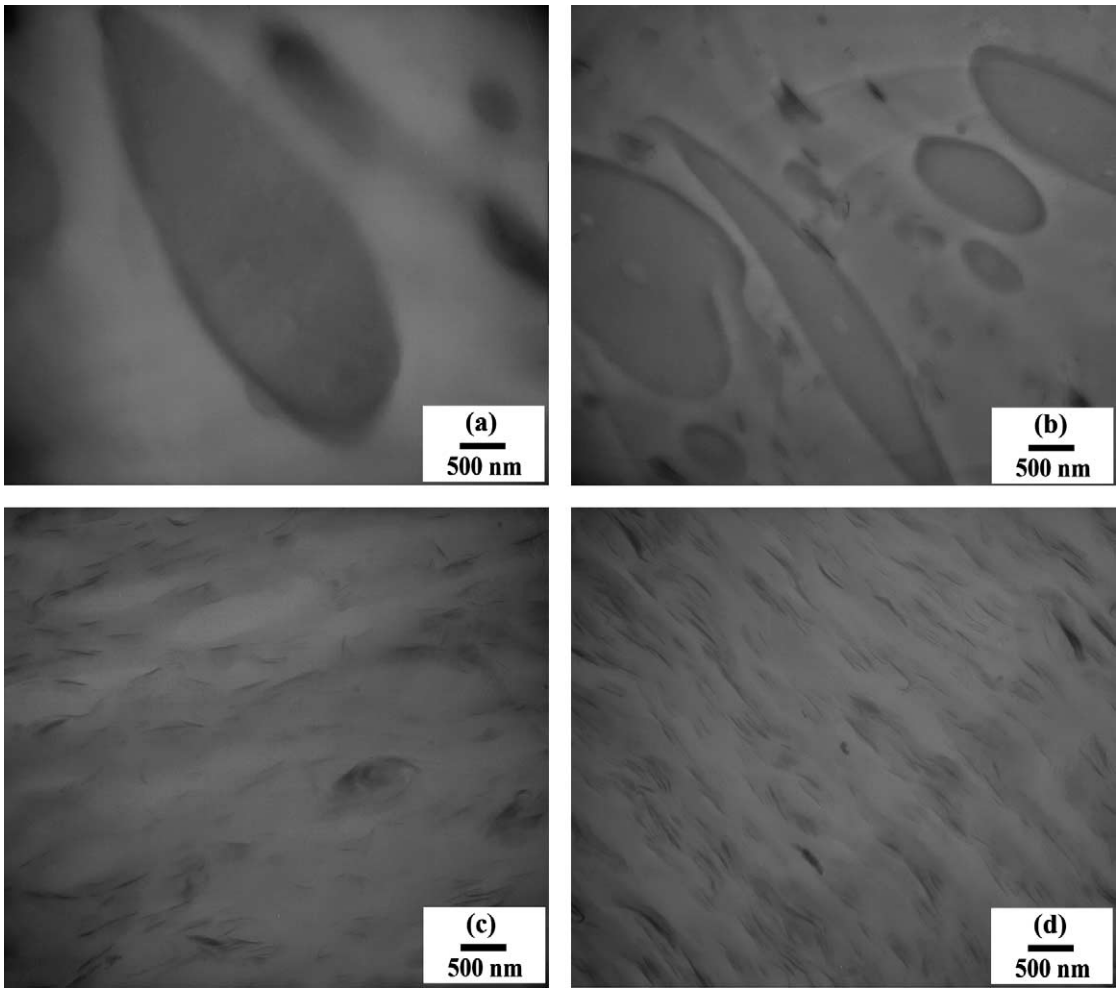

Fig. 6. TEM micrographs of PP/elastomer/masterbatch nanocomposites showing rubber particle morphology. The materials contain 30 wt% elastomer and the following MMT contents: (a) 0 wt%, (b) 1 wt%, (c) 2.8 wt% and (d) 6.8 wt%. Images were taken from the core and viewed parallel to the TD.

the clay particles, and the elastomer particles can be easily identified by TEM. On further addition of MMT, there is an even more dramatic change in the morphology. Fig. 6(c) shows a TEM micrograph for a nanocomposite containing 30 wt% elastomer and 3 wt% MMT. The identification of the elastomer particles in the TEM micrographs is now more difficult. The elastomer particles appear to be much smaller and comparable to those of clay platelets, e.g. a few hundreds nanometers. Thus, differentiation between the clay platelets and elastomer particles becomes more difficult. These effects are even more pronounced in nanocomposites containing 7% MMT and 30% elastomer as shown in Fig. 6(d).

The characterization of elastomer particles, e.g. size, shape and distribution etc., for these nanocomposites is quite important since the toughening behavior of polymer nanocomposites and/or blends is highly dependent on the morphology of the elastomer phase [33,34]. TEM micrographs, like those shown already, can provide only limited information about the elastomer phase due to the relatively small observable area at the magnifications needed to see the clay particles. The usefulness of AFM for investigation of clay particles in nanocomposites is still in question and may be dependent on the matrix material. On the other hand, identifying elastomer particles using AFM in PP/elastomer/filler nanocomposites is relatively easy and simple. A sizable difference in the stiffness of the components at the sample surface can provide images with higher phase contrast; this is ideal for polyolefin/elastomer systems where staining of one component but not the other for TEM characterization is quite difficult due to the similar chemical structure of both components, e.g. PP and ethylene–octene based elastomer.

Fig. 7 shows a series of AFM images for PP/elastomer/masterbatch nanocomposites containing 30% elastomer and various amounts of MMT, which were viewed parallel to the FD. In these AFM images, soft elastomer particles appear dark while the relatively stiffer PP matrix appears bright. As seen in Fig. 7(a), elastomer particles with the size of a few μm were observed for the PP/elastomer blend with no clay. The addition of 1 wt% MMT to the PP/elastomer blend leads to an apparent reduction in the size of the elastomer particles as shown in Fig. 7(b). It should be noted that the plane of viewing for the AFM images (viewed parallel to FD, or TD–ND plane) in Fig. 7 is different from that for the TEM micrographs (viewed parallel to TD, or FD–ND plane) in Fig. 6; so, it is expected that

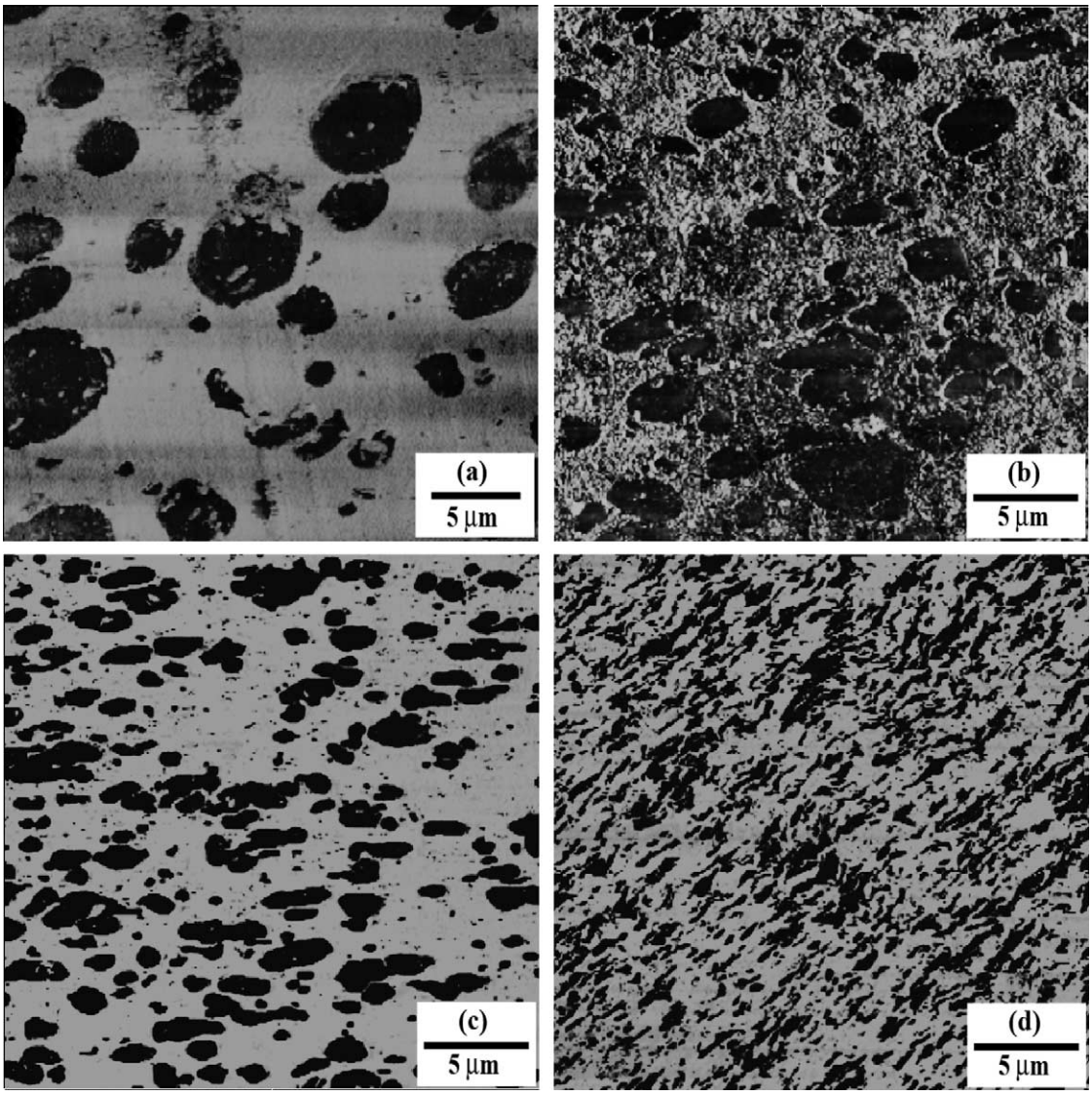

Fig. 7. AFM images of PP/elastomer/masterbatch nanocomposites to reveal rubber particle morphology. The materials contain 30 wt% elastomer and the following MMT contents: (a) 0 wt%, (b) 1 wt%, (c) 2.8 wt% and (d) 6.8 wt%. The Images are of a microtomed surface in the TD–ND plane taken from the specimen core.

the elastomer particles in the TEM micrographs in Fig. 6 would appear as more elongated shapes than in the AFM images in Fig. 7. Further addition of more than 1 wt% MMT leads to dramatic changes in the morphology of these nanocomposites, see Fig. 7 (c) and (d). In nanocomposites containing 30 wt% elastomer and 2.8 wt% MMT, the elastomer particles are relatively well dispersed in the PP matrix with smaller size and more elongated shape than those in nanocomposites containing lower contents of MMT as shown in Fig. 7(c). AFM images of nanocomposites containing 6.8 wt% MMT reveal much smaller elastomer particles with a more irregular shape. These apparent changes in the morphology of the elastomer phase, e.g. decreasing in size and increasing irregularity in particle-shape, may stem from two competing effects during melt-processing; one is rheological in origin while the other stems from a 'barrier' effect of the clay particles on rubber particle coalescence. The literature shows that addition of clay to a polymer melt causes an increase in the viscosity [35–38]. The melt viscosity ratio of the elastomer phase to that of the matrix and the absolute viscosity of the matrix are important factors that control the elastomer particle breakup during melt processing. In principle, an increase in matrix viscosity can alter the balance of drop breakup versus coalescence in such a way as to produce smaller rubber particles [39]. In addition, Kim et al. have suggested that the presence of clay particles retards the coalescence of small elastomer particles to form larger ones resulting in a net reduction in the elastomer particle size. Their work on the morphology of nylon/EPR rubber/clay nanocomposites demonstrated that dispersed clay particles caused a reduction in the size and stability of the dispersed elastomer domains in a nylon 6 matrix via this 'barrier' to coalescence mechanism [40]. We believe this retardation of rubber particle coalescence by clay particles is a major factor in the reduction in elastomer particle size seen here.

Fig. 8 shows schematically the morphological change in PP/elastomer composites occurs with the addition of clay based on

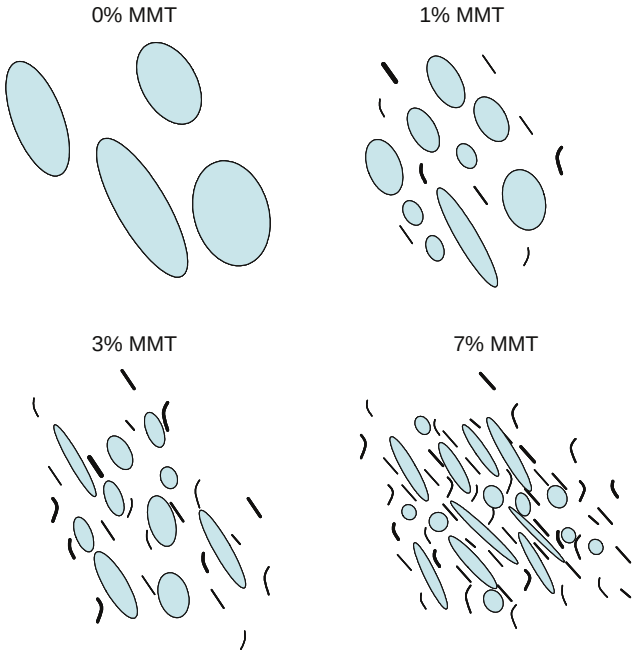

Fig. 8. Schematic illustration of the morphological change in PP/elastomer/-masterbatch nanocomposites with increasing MMT content at a fixed elastomer concentration.

the TEM and AFM observations shown above. This reduction in the size of the elastomer particle is believed to be responsible for the improved toughening, described later for nanocomposites containing high content of elastomer, as MMT is added to the blends. To address the effect of clay particles on the size of elastomer particles, a quantitative analysis of elastomer particle size was made from a number of AFM images as described in the next section.

3.2. Particle analyses for PP/elastomer/masterbatch nanocomposites

3.2.1. Clay particle analysis

For best statistical validity, a substantial number of particles should be analyzed for a given nanocomposite, e.g. order of 400–500 particles. However, this is difficult, especially for less exfoliated nanocomposites containing low concentrations of the filler. For this analysis, the length and thickness of 100–300 particles were determined for PP/masterbatch nanocomposites containing 1, 2.8 and 6.8 wt% MMT.

Fig. 9 shows a series of histograms of MMT particle lengths and pertinent statistical data obtained on PP/masterbatch nanocomposites containing 1, 2.8 and 6.8% MMT. The sections were taken from the core region of injection molded specimens and viewed parallel to the TD so that the measurements were performed on particles presented in the FD–ND plane. Similar measurements were conducted for the thickness of clay particles and the results are plotted in Fig. 10. As seen in these histograms, there exists a sizeable distribution in both particle length and thickness. The average particle length tends to decrease with increasing MMT content, while the particle thickness increases; Fig. 11 shows these trends of

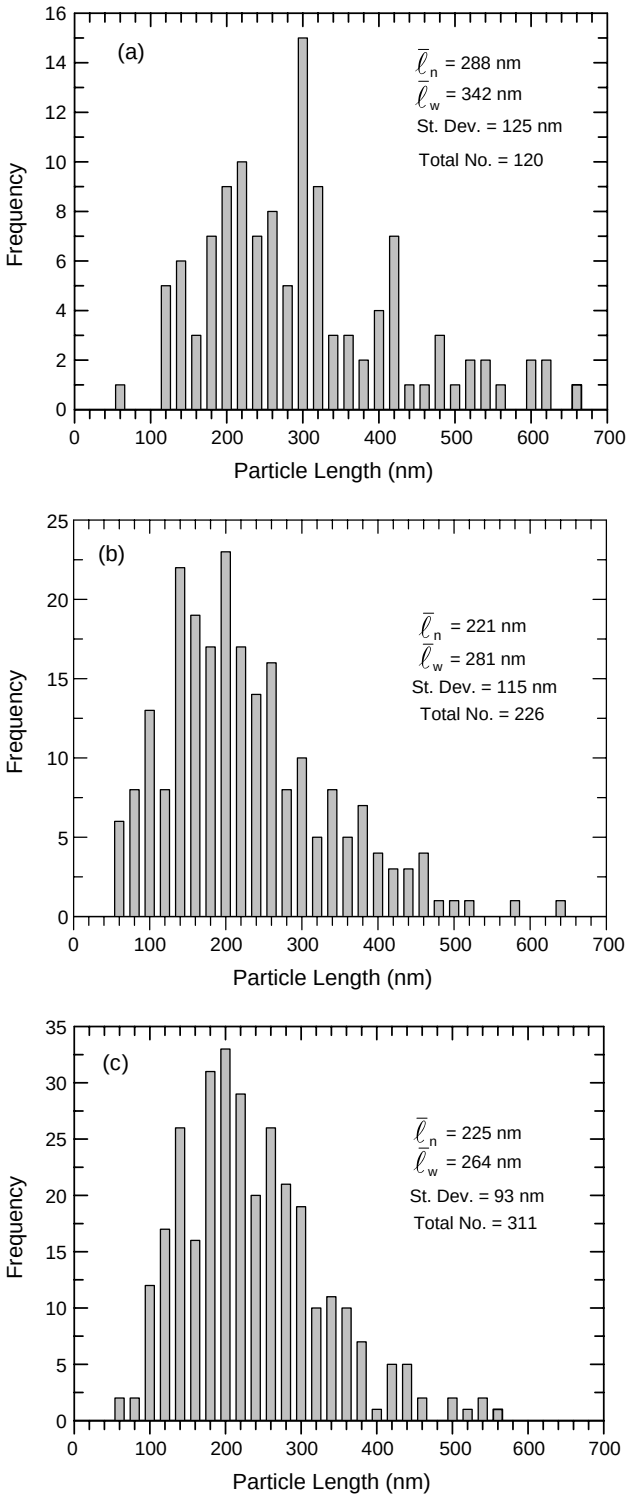

Fig. 9. Histograms of MMT particle length obtained by analyzing TEM micrographs of PP/masterbatch nanocomposites containing the following MMT contents: (a) 1 wt%, (b) 2.8 wt% and (c) 6.8 wt%. Photomicrographs used for analysis were taken from the core and viewed parallel to the TD.

length and thickness (Fig. 11(a)) and their particle aspect ratio (Fig. 11(b)), i.e. their length/thickness. The average particle length decreases sharply as MMT content changes from 1 to 2.8 wt%; however, further addition of the MMT does not have a large effect on particle length. On the other hand, the average

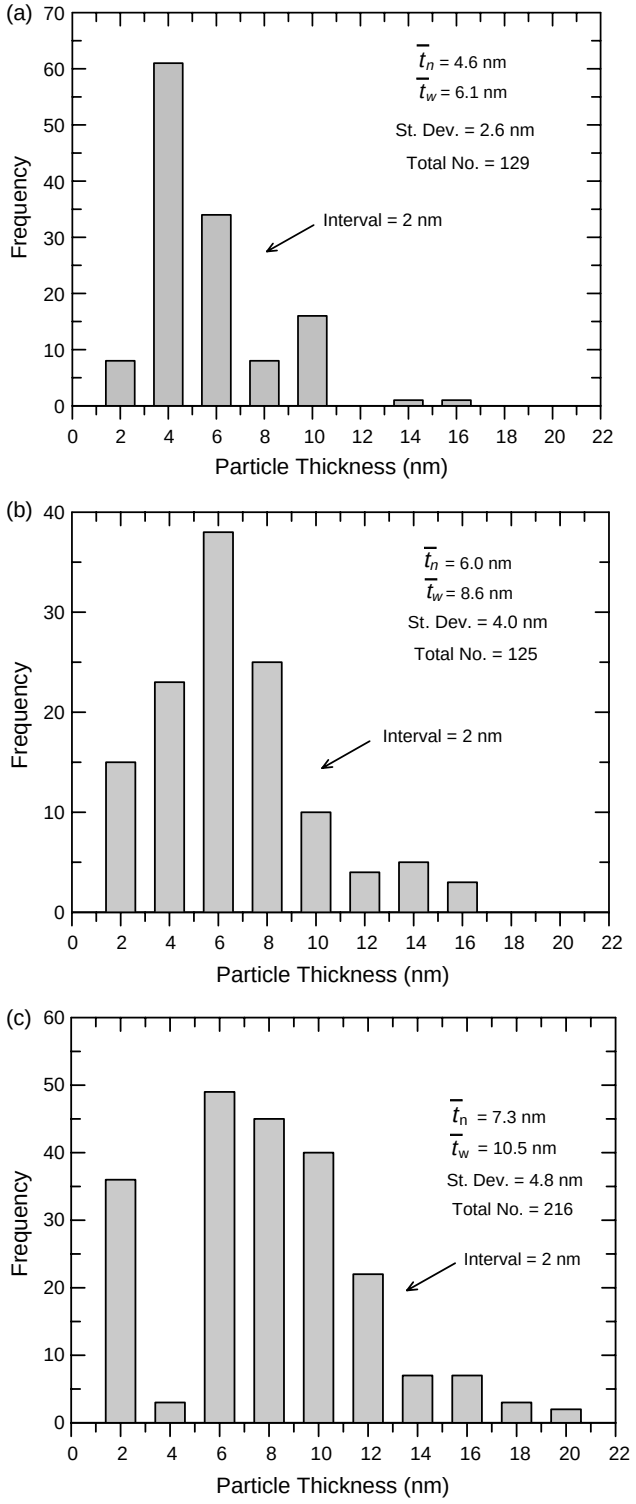

Fig. 10. Histograms of MMT particle thickness obtained by analyzing TEM micrographs of PP/masterbatch nanocomposites containing the following MMT contents: (a) 1 wt%, (b) 2.8 wt% and (c) 6.8 wt%. Photomicrographs used for analysis were taken from the core and viewed parallel to the TD.

particle thickness continues to increase with increasing MMT concentration. As a result, the average aspect ratio decreases rapidly in going from 1 to 2.8 wt% MMT and then decreases slightly more with further addition of MMT. Interestingly, Nam et al. reported similar trends of changing particle length

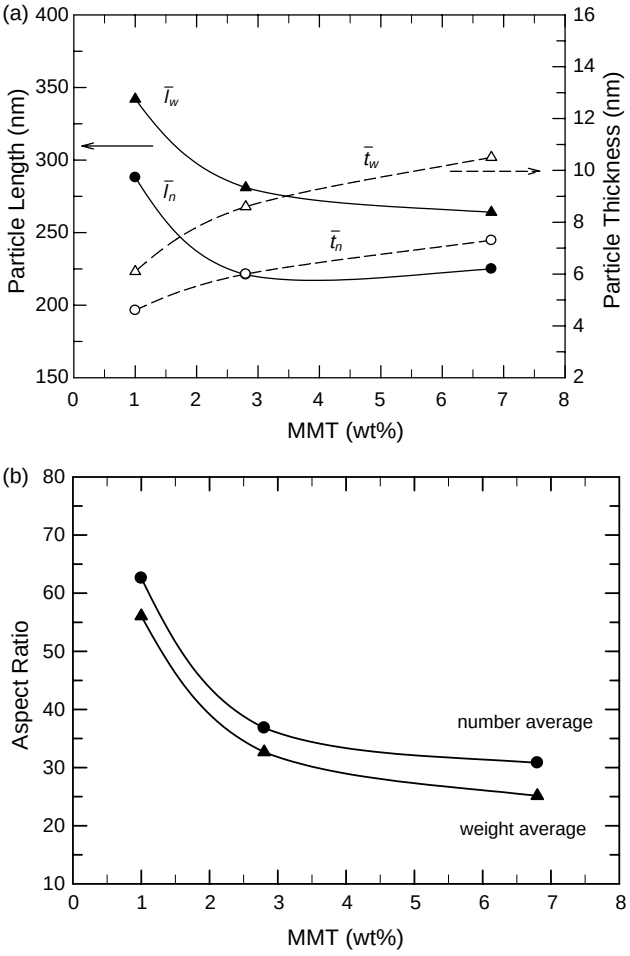

Fig. 11. The effect of MMT levels on (a) particle length and thickness and (b) aspect ratio of PP/masterbatch nanocomposites.

and thickness with varying of MMT contents in PP-*g*-MA/clay nanocomposites [41]; however, their reported range of particle lengths is somewhat shorter than that from the present study. Analysis of TEM images for PP/masterbatch nanocomposites are summarized in Table 1.

Quantification of the dimensions of clay particles in polymer nanocomposites has been the subject of increasing interest and some debate in recent times. A number of studies have attempted to measure the lengths of individual clay platelets using several techniques such as TEM and AFM [29, 32]. However, even for in situ polymerized nanocomposites,

Table 1
Image analysis results obtained on TEM micrographs of injection molded PP/masterbatch nanocomposites

	Viewed parallel to TD		
MMT concentration (wt%)	1.0	2.8	6.8
Number average particle length $\bar{l}_n$ (nm)	288	221	225
Weight average particle length $\bar{l}_w$ (nm)	342	281	264
Number average particle thickness $\bar{t}_n$(nm)	4.6	6.0	7.3
Weight average particle thickness $\bar{t}_w$ (nm)	6.1	8.6	10.5
Particle aspect ratio, $\bar{l}_n/\bar{t}_n$	63	37	31
particle aspect ratio, $\bar{l}_w/\bar{t}_w$	56	33	25

different clay particle lengths were reported when the clay from the same source was used in nanocomposites [42,43].

For melt-processed nanocomposites, the stress field within the mixing device creates smaller particles from larger ones; for polymers that have good affinity for the organoclay, like nylon 6, there is an evidence of peeling away of individual platelets from these particles as the ultimate step in the evolution toward complete exfoliation [36]. When the polymer affinity for the organoclay is not good enough to create a preponderance of individually dispersed platelets, the morphology achieved is dominated by the processes involved in the break down of large particles into smaller ones and these mechanisms are not well understood at this time. It is not clear yet whether this simply involves deaggregation of bundles of platelets into smaller particles or whether the platelets of montmorillonite are actually broken or attrited during mixing. The result in Fig. 11 shows that particle size evolution, by whatever mechanism, is affected by the content of organoclay in the mixture. We can expect that higher filler loadings increase the mixture viscosity and, hence the stresses during mixing. In addition, higher loading increases the particle–particle interactions during mixing. Evidently, the consequence of these effects, and possibly others, during particle break down is to decrease particle length but also to increase particle thickness, see Fig. 11(a). Whatever the mechanistic details of this may be, the net effect is a decrease in particle aspect ratio with loading, see Fig. 11(b); this means that property enhancements are not as large at high loadings as would be expected from trends at low loading. It would be useful to better understand this behavior and to find ways to increase aspect ratios, especially at higher loadings.

As shown in Fig. 3(a), the PP-*g*-MA/organoclay masterbatch contains clay platelets as an intercalated bundle, which may be dispersed more easily into the PP matrix, with the help of PP-*g*-MA, at low MMT concentrations than at higher concentrations. For example, at 7 wt% MMT, some bundles of the clay platelets may prefer to stay embedded in PP-*g*-MA, resulting in an increase in the average thickness of the clay particles. Some of the factors that may contribute to the poorer dispersion of the clay particles at high loading include the difference in rheological properties of the masterbatch and the base PP, the extent of compatibility between PP and PP-*g*-MA, and the extent of clay dispersion in the masterbatch. Selection of other PP-*g*-MA materials, e.g. different MA content, and optimizing the masterbatch formulation may be key to improving the dispersion of clay platelets in nanocomposites containing high MMT concentrations.

TEM micrographs used in this particle analysis study were taken from a view parallel to the TD (FD–ND plane); however, TEM images obtained from different viewing planes, i.e. parallel to the FD and ND, revealed that dispersed clay particles have an anisotropic disk-like nature in shape, i.e. different length along the FD and TD directions, such that the particle cannot be fully described by just an aspect ratio. The alignment of anisotropic clay particles along the flow direction may lead to a significant directional difference in mechanical and thermal properties. The effect of an anisotropic nature of the filler for these nanocomposites will be discussed in more detail in the thermal expansion part of subsequent papers.

Although the relatively small number of particles used for this image analysis may limit the statistical confidence in the data, the average aspect ratios obtained from the image analyses here successfully explain, at least in a semi-quantitative way, the stiffness behavior of PP/masterbatch nanocomposites when compared with conventional composite theories; these results will be addressed in subsequent papers.

3.2.2. Elastomer particle analysis

Particle analysis for the elastomer phase in PP/elastomer/-masterbatch nanocomposites is quite complex due to the nonspherical nature of the particles as shown in the AFM images, see Fig. 7. To determine the size of elastomer particles, the image analyzing software used identifies each individual elastomer particle and evaluates its area, A, and lengths along the major and minor axes. For simple comparison among nanocomposites, an apparent elastomer particle size, d, was calculated using the following relation.

$$d = \left(\frac{4A}{\pi}\right)^{1/2} \tag{1}$$

A series of histograms of apparent elastomer particle sizes defined by Eq. (1), see Fig. 12, and lengths (not shown here) was built for the nanocomposites containing 30 wt% elastomer and various amounts of MMT. From the distribution of elastomer particle sizes shown in the histograms, the number and weight average apparent particle size, d, and average length, l, values along the major and minor axes are calculated as follows

$$\bar{d}_{\mathrm{n}} = \frac{\sum n_i d_i}{\sum n_i}, \quad \bar{l}_{\mathrm{n}} = \frac{\sum n_i l_i}{\sum n_i} \tag{2}$$

$$\bar{d}_{\mathrm{w}} = \frac{\sum n_i d_i^2}{\sum n_i d_i}, \quad \bar{l}_{\mathrm{w}} = \frac{\sum n_i l_i^2}{\sum n_i l_i} \tag{3}$$

where n_i is the number of elastomer particles within fixed increments of d_i and l_i. No attempt was made to convert apparent particle sizes into true particle sizes due to the complex nature of the particle shape. The interparticle distance, ID, sometimes referred to as the matrix ligament thickness, can be calculated from the following equation [44]

$$\mathrm{ID} = d\left[\left(\frac{\pi}{6\phi_{\mathrm{r}}}\right)^{1/3} - 1\right] \tag{4}$$

where ϕ_{r} is the dispersed particle volume fraction and d is the average particle diameter. The apparent particle size, $\bar{d}_{\mathrm{w}}$, was used to calculate the ID shown in Table 2.

Table 2 summarizes the elastomer particle size analyses for a series of nanocomposites containing 30 wt% elastomer with 0 to 6.8 wt% of MMT. Fig. 13 shows the number and weight average apparent particle sizes plus interparticle distances (ID) between elastomer particles as a function of MMT content. The average particle size decreases rapidly with addition of 1 wt% of MMT and then more gradually with further increases in

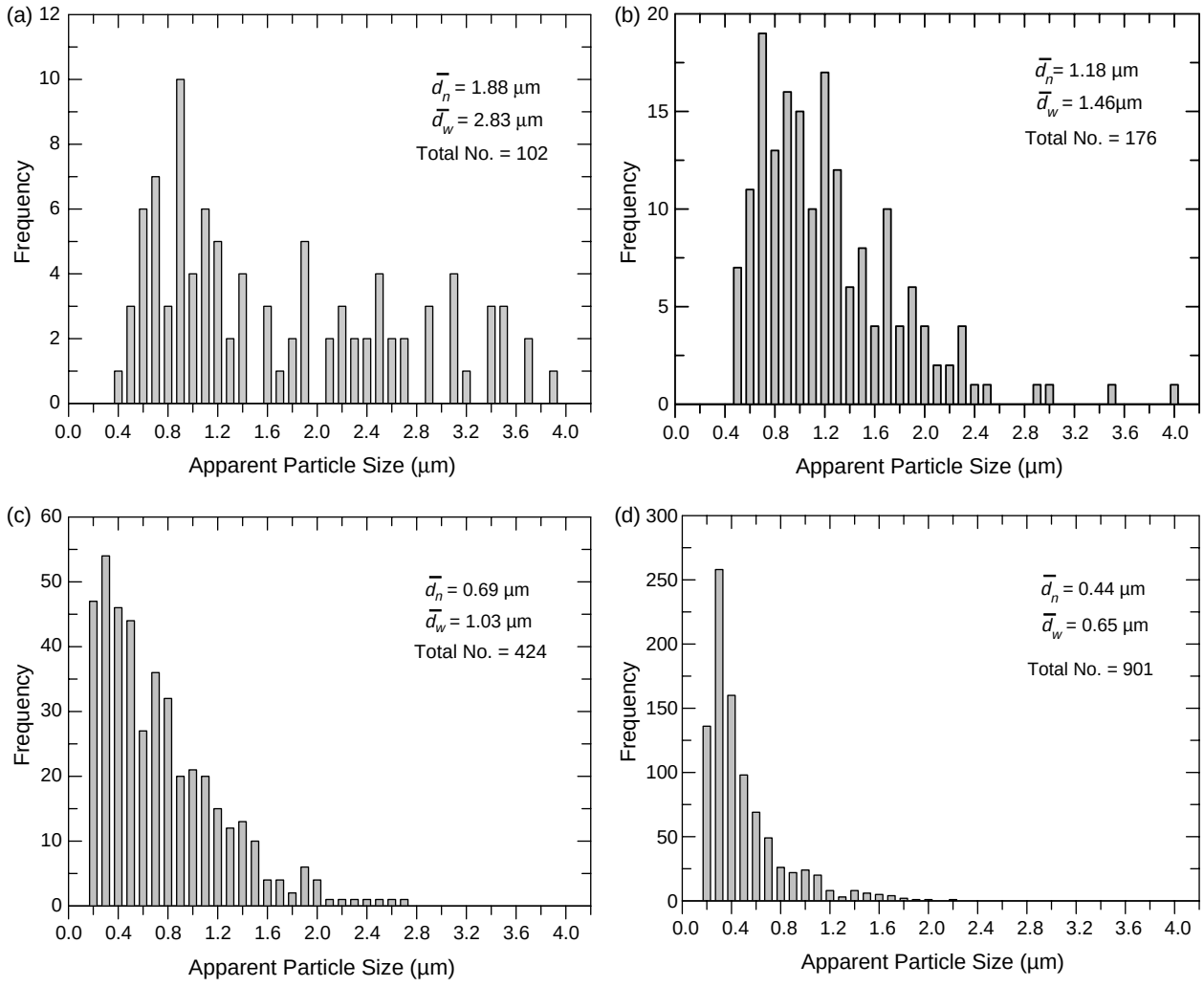

Fig. 12. Histograms of apparent elastomer particle size data obtained by analyzing AFM images of PP/elastomer/masterbatch nanocomposites containing 30 wt% elastomer and the following MMT contents: (a) 0 wt%, (b) 1 wt%, (c) 2.8 wt% and (d) 6.8 wt%. AFM images used for analysis were taken from the core and viewed parallel to the FD.

MMT content. Similar trends are observed for the interparticle distance.

The similar trends in average lengths along the major and minor axes of the elastomer particles are also apparent, i.e. a rapid decrease with addition of clay and then, a gradual decrease with further addition of MMT. For blends, it is generally recognized that as the dispersed particles become smaller in size, it is much more difficult for them to take on elongated shapes due to interfacial tension considerations. However, the elastomer particle aspect ratio, i.e. major length/minor length of a particle, increases as the apparent particle size decreases for the current nanocomposites. This may stem from the nature of the 'barrier' effect induced by the presence of the clay particles which become oriented along the flow field generated by the injection molding process. These deformed elastomer particles within the injection molded specimens may have a more important role in the thermal expansion behavior than in the mechanical properties for nanocomposites where the directional dependence of the properties is greater in any case. The directional differences

Table 2
Elastomer particle size comparison for PP/elastomer/masterbatch nanocomposites containing 30% elastomer for different MMT contents

MMT (wt%)	Major length (μm)		Minor length (μm)		$\bar{d}_n$ (μm)	$\bar{d}_w$ (μm)	ID (μm)	Elastomer aspect ratio (major/minor)	
	$\bar{l}_n$	$\bar{l}_w$	$\bar{l}_n$	$\bar{l}_w$				$\bar{l}_{n,major}/\bar{l}_{n,minor}$	$\bar{l}_{w,major}/\bar{l}_{w,minor}$
0	2.38	3.55	1.56	2.46	1.88	2.83	0.55	1.5	1.4
1	1.64	2.14	0.89	1.1	1.18	1.46	0.28	1.8	2.0
2.8	1.08	1.94	0.52	0.77	0.69	1.03	0.20	2.1	2.5
6.8	0.88	1.66	0.32	0.58	0.44	0.65	0.13	2.8	2.9

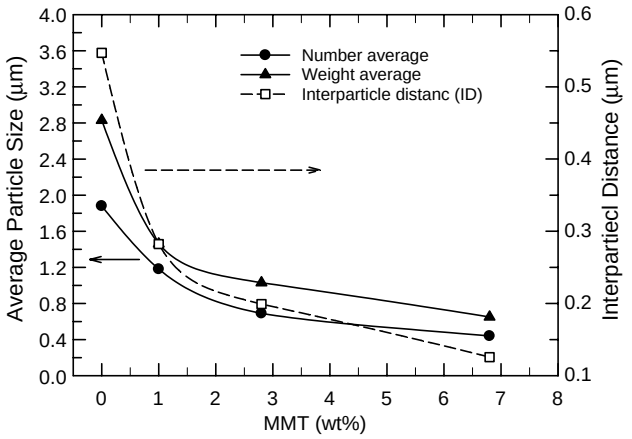

Fig. 13. The effect of MMT levels on the number and weight average apparent elastomer particle sizes (filled symbols) and interparticle distance (open symbol) of PP/elastomer/masterbatch nanocomposites containing 30 wt% elastomer.

in the size, size distribution and shape of the clay and elastomer particles in the morphology of these nanocomposites will be discussed in more detail in subsequent papers dealing with thermal expansion behavior.

A mechanical brittle–ductile transition generally can be induced either by increasing elastomer content or decreasing elastomer particle size. A number of studies on the toughening behavior of PP/rubber composites have suggested that in addition to dispersed particle size and content, interparticle distance or matrix ligament thickness is an important morphological parameter that affects the brittle–ductile transition of these systems [34,44,45]. However, the distance between elastomer particles is much more difficult to define than the apparent particle size for the current nanocomposites due to their complex morphology as revealed by AFM.

As will be shown later, the fracture behavior of nanocomposites containing 30 wt% elastomer undergoes a brittle–ductile transition as the amount of MMT changes from 1 to 2.8 wt%; the nanocomposite containing 2.8 wt% of MMT is super-tough (>600 J/m) while the one containing 1 wt% of MMT is relatively brittle (~ 100 J/m). This apparent toughening may be attributed to the decrease in the elastomer particle size and/or interparticle distance to below a critical value that induces the brittle–ductile transition [44,46]. Jiang et al. reported that the brittle–ductile transition for the blends of PP, nylon 66 and HDPE with rubber is dependent on the interparticle distance, temperature, testing speed and matrix properties [46,47]. For their PP/EPDM blends, the average particle size remained fixed regardless of the amount of the rubber in the system, e.g. 0.5–0.8 μm; however, increasing the rubber content led to a decrease in the interparticle distance, which resulted in an apparent toughening for PP/rubber blends. They reported a critical value of interparticle distance at 25 °C of 0.15 μm for PP/EPDM blends. The critical value for the brittle–ductile transition for their PP/EPDM blends may not be exactly the same as that for the current PP/elastomer/masterbatch nanocomposites since the toughening mechanism for PP/rubber blends is known to be dependent on the rubber characteristics used [26]. For the current nanocomposites, the elastomer particle size decreases with increasing filler content. The elastomer particle analysis shown in Table 2 suggests that the critical value of apparent particle size for toughening lies between 1.5 and 1.0 μm and that the critical interparticle distance is of the order of 0.3–0.2 μm; however, these values should be considered as relative ones since true particle sizes cannot be easily obtained due to the complex nature of the particle shape for these nanocomposites.

3.3. WAXD scans for nanocomposites

Fig. 14 compares WAXD scans for the organoclay used to form the masterbatch with scans for PP nanocomposites, without elastomer, made by the mixing PP with the masterbatch in various proportions in order to achieve different MMT contents in the final composite. The neat organoclay shows an intense peak at around $2\theta = 3.6°$, corresponding to a basal spacing of 24.2 Å. The scans taken from the core portion of the injection molded specimen, see Fig. 14(a), do not show a characteristic basal reflection for all MMT concentrations; this might be interpreted to mean that organoclay is well dispersed as individual platelets in the matrix, i.e. an exfoliated structure, and that exfoliation increases at higher MMT contents since the broad peak at 1 wt% MMT gradually disappears as the MMT content increases. These suggestions, however, are opposite to the results from the TEM particle analysis in Section 3.2 which show that the level of dispersion, i.e. aspect ratio of clay particles, decreases with increasing MMT concentration. However, the WAXD scans from the skin portion, Fig. 14(b), reveal that a strong peak from the organoclay persists in these nanocomposites without any significant shift in location; however, the intensity of this peak increases with increasing MMT content, indicating that large stacks of platelets exist in the skin portion of injection molded specimens. This suggests distinct differences in structure between the skin and core regions of injection molded Izod bars. The injection molding process changes not only the characteristics of the clay peak, e.g. strong intensity in the skin and absence of a peak in the core, but also of the crystalline characteristics of the PP matrix. Fig. 14(c) and (d) show WAXD scans at higher angles where the PP crystalline structure is revealed in a corresponding fashion as Fig. 14(a) and (b) for the clay region. The X-ray scans from the core region do not show any significant differences in PP crystalline structure with varying amounts of MMT, Fig. 14(c); whereas, the addition of clay results in a striking change in the PP WAXD scans in the skin portion. The ratio of the intensity of the (040) reflection, corresponding to a peak at $2\theta = 16.9°$, and the (110) reflection, corresponding to a peak at $2\theta = 14.1°$, $[I_{040}/I_{110}]$ is often used to evaluate the degree of crystal orientation. The increase in the diffraction intensity of the (040) reflection compared to the (110) reflection indicates that the lamellar crystals are preferentially oriented perpendicular to the flow direction within an Izod bar, suggesting that the extent of the transcrystals increases from the core to skin region.

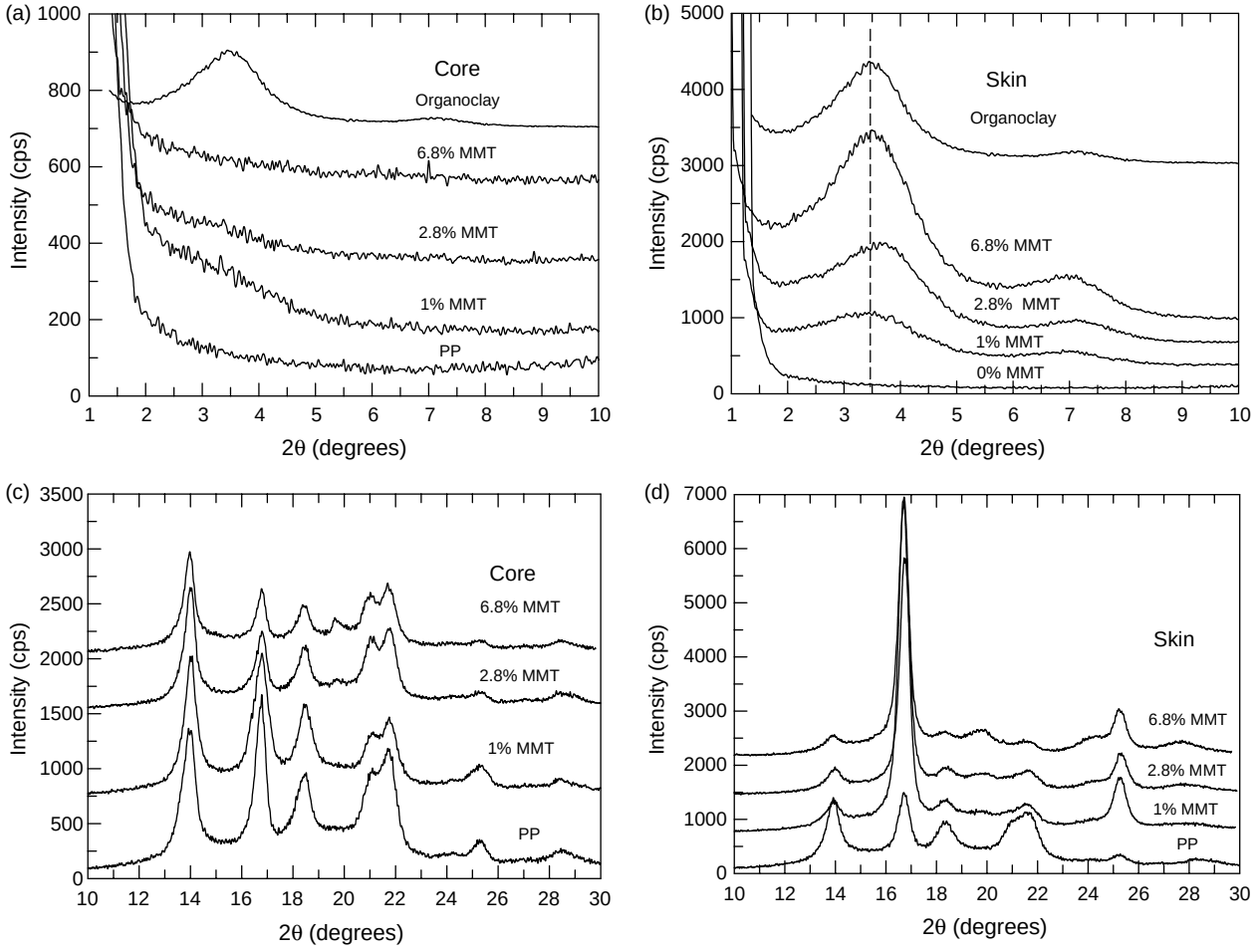

Fig. 14. WAXD scans for organoclay used for masterbatch and PP/masterbatch nanocomposites containing 1, 2.8 and 6.8 wt% MMT. The low angle region reveals MMT morphology taken from the core (a) and from the skin (b), while the high angle region reveals the PP crystal structure taken from the core (c) and from the skin (d). The curves are shifted vertically for clarity.

The absence of a clay peak in the core region compared to the skin might possibly stem from differences in volumes of material that the X-ray beam encounters. However, as shown in Fig. 14(c), WAXD scans from the PP crystal region show similar intensities for the polypropylene peaks, indicating that the volume sampled in the two types of scans is nearly the same.

The intensity differences of the characteristic peaks of the clay could possibly stem from differences in the degree of exfoliation of clay from the core to skin and/or difference in the orientation of clay particles in these regions during the injection molding process. There is little mechanistic reason to believe that exfoliation varies across from the skin to core regions. So, it is believed that there is a significant difference in the orientation of clay particles in the skin and core regions in the injection-molded specimen. Also, the WAXD scans indicate that the clay dispersion and/or orientation has significant effects on the orientation of the PP crystals. This skin–core effect is particularly of interest from the industrial point of view, since the injection molding process is largely involved in the production of commercial products. A subsequent publication will explore the skin–core effect observed for these nanocomposites in more detailed ways.

Fig. 15 shows WAXD scans for the nanocomposites containing 30 wt% elastomer and various amounts of MMT in a corresponding fashion as Fig. 14. A similar skin–core effect is apparent for the nanocomposites containing elastomer; however, the implied trends for the clay dispersion in the core region are opposite of that for nanocomposites containing no elastomer, i.e. a broad peak becomes distinct with increasing MMT content; this would be indicative of the presence of a sizable fraction of unexfoliated clay particles. Also, the intensity of the clay peak in the skin portion from these nanocomposites is somewhat lower than that from PP/masterbatch nanocomposites. This suggests that the degree of exfoliation, distribution and/or orientation of clay particles in the core and skin regions are clearly affected by the addition of elastomer. The X-ray scans indicate that incorporating of elastomer may lead to a lower extent of exfoliation of clay particles in these nanocomposites. Indeed, TEM images for the nanocomposites containing higher elastomer contents show less exfoliation and dispersion of clay particles; however,

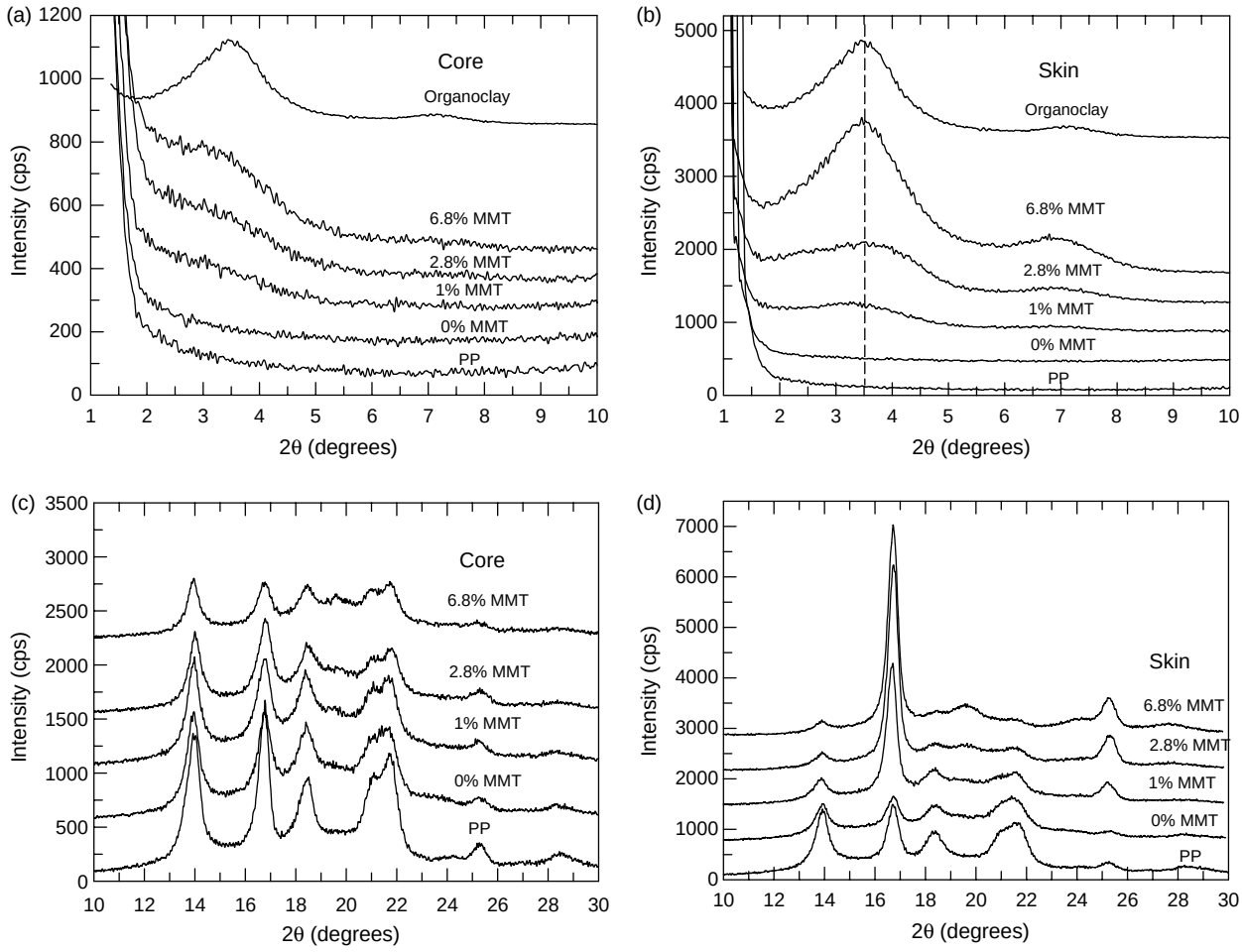

Fig. 15. WAXD scans for the PP/elastomer /masterbatch nanocomposites containing 30 wt% elastomer and 1, 2.8 and 6.8 wt% MMT. The low angle region reveals MMT morphology taken from the core (a) and from the skin (b), while the high angle region reveals the PP crystal structure taken from the core (c) and from the skin (d). The curves are shifted vertically for clarity.

a detailed quantitative particle analysis for the nanocomposites containing elastomer using TEM is quite difficult due to an apparent heterogeneous distribution of clay particles, a contrast interference between the clay and elastomer particle and the fact that the elastomer phase is very unstable under the TEM electron beam prevents obtaining higher quality TEM images.

3.4. Mechanical properties

Fig. 16 shows the effect of MMT and elastomer content on the modulus of these nanocomposites. The addition of MMT to PP containing no elastomer results in a substantial increase in stiffness at low MMT concentrations, i.e. $<$2–3 wt%, while the rate of increase at higher clay concentrations is less pronounced. Similar trends are evident for PP/elastomer/masterbatch nanocomposites. The particle analyses for the clay particles indicate that the lower reinforcing efficiency at higher concentrations of MMT can be attributed to the lower aspect ratio of clay particles at higher clay contents. However, effects of other factors such as reduced platelet orientation and/or the increased amount of PP-*g*-MA, whose modulus is considerably less than that of pure PP, may not be ruled out. With regard to the latter effect, PP-*g*-MA is needed to achieve the better dispersion of silicate platelets in PP matrix and, as a consequence, improved stiffness of PP nanocomposites; however, very few studies have been reported in the literature regarding how the ratio of organoclay to PP-*g*-MA affects morphology and performance of PP-based nanocomposites [2,48]. This subject will be explored in more detail in future investigations in this laboratory. Flexural modulus of the PP/elastomer/masterbatch nanocomposites, see Fig. 16(b), exhibits similar trends as the tensile modulus.

Fig. 17 shows the influence of MMT and elastomer content on yield strength for PP/masterbatch and PP/elastomer/masterbatch nanocomposites. Yield strength and elongation at yield and break values are reported separately for both nanocomposites since PP/masterbatch nanocomposites were tested at a lower crosshead speed and broke prior to yielding at higher MMT concentrations, e.g. $>$3 wt%, as shown in Fig. 17(a) and 18(a). Unlike the modulus, adding MMT to PP and PP/elastomer composites results in a marginal increase in yield strength with addition of MMT and, as expected, adding elastomer decreases the yield strength of

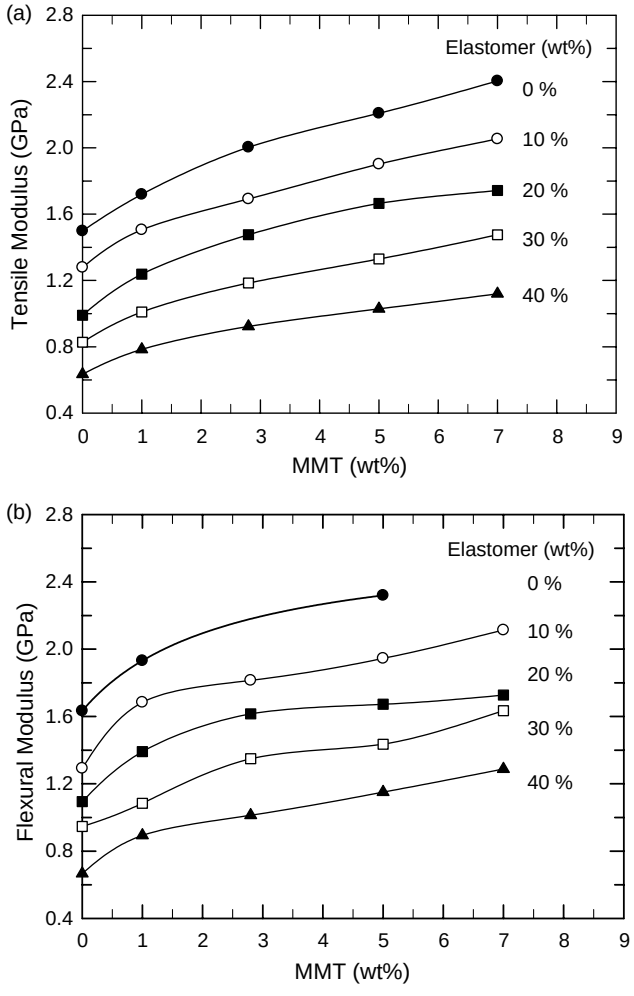

Fig. 16. Effect of MMT and elastomer content on (a) the tensile modulus and (b) the flexural modulus of PP/elastomer/masterbatch nanocomposites.

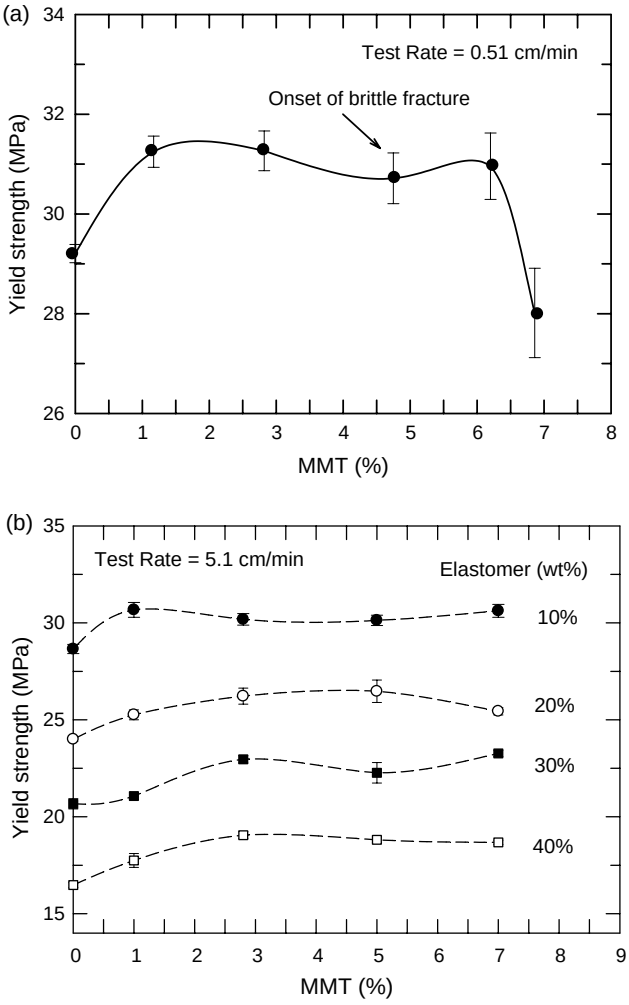

Fig. 17. Effect of MMT and elastomer content on the yield strength of (a) PP/masterbatch with no elastomer (test speed = 0.51 cm/min) and (b) PP/elastomer/masterbatch nanocomposites (test speed = 5.1 cm/min).

the nanocomposites. Addition of MMT beyond ~1 wt% does not significantly change the yield strength of these nanocomposites.

The elongation at yield for PP/masterbatch and PP/elastomer/masterbatch nanocomposites are shown graphically in Fig. 18. The nanocomposites without elastomer were tested at a lower crosshead speed of 0.51 cm/min and the elongation at yield decreases with increasing the amount of MMT and failed in a brittle manner at higher MMT contents. However, adding MMT to PP/elastomer composites shows rather different elongation behavior depending on the elastomer concentration as seen in Fig. 18(b). For nanocomposites containing 10 wt% elastomer, the elongation at yield decreases sharply with the addition of MMT and then decreases slightly as MMT loading increases. Similarly, the addition of small amounts of MMT, e.g. 1 wt%, leads to a drop in the elongation at yield for nanocomposites containing 20 and 30 wt% elastomer; however, the values increase with further increasing of MMT content. The elongation at yield for nanocomposites containing 40 wt% of elastomer increases slightly as the amount of MMT increases. The elongation at break data have a relatively large standard deviation as shown in Fig. 19. However, it is clear that increasing elastomer amount results in higher values of elongation at break and, as expected, the addition of MMT leads to a significant decrease in elongation at break. For nanocomposites containing 20 wt% elastomer, the elongation at break decreases significantly with the addition of MMT and exhibits similar values as nanocomposites containing 10 wt% elastomer. On the other hand, for nanocomposites containing higher amounts of elastomer, e.g. 30 and 40 wt%, elongation at break remains relatively high at higher MMT concentrations. This is most likely due to the fine dispersion of elastomer phase with smaller particle size in the nanocomposites containing higher amounts of MMT and elastomer as revealed in Fig. 7.

Fig. 20 shows the influence of MMT and elastomer content on notched Izod impact strength. For nanocomposites containing up to 20 wt% elastomer, the addition of MMT leads to a decrease in the Izod values for nanocomposites with no elastomer or a slight increase for

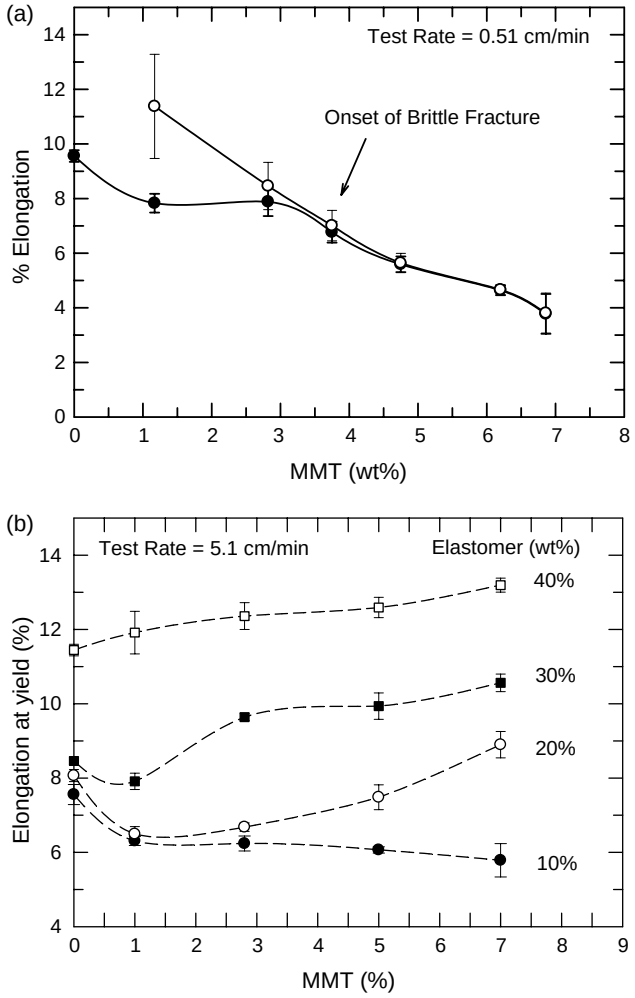

Fig. 18. Effect of MMT and elastomer contents on (a) the elongation at yield and break of PP/masterbatch with no elastomer (test speed = 0.51 cm/min) and (b) the elongation at yield of PP/elastomer/masterbatch nanocomposites (test speed = 5.1 cm/min).

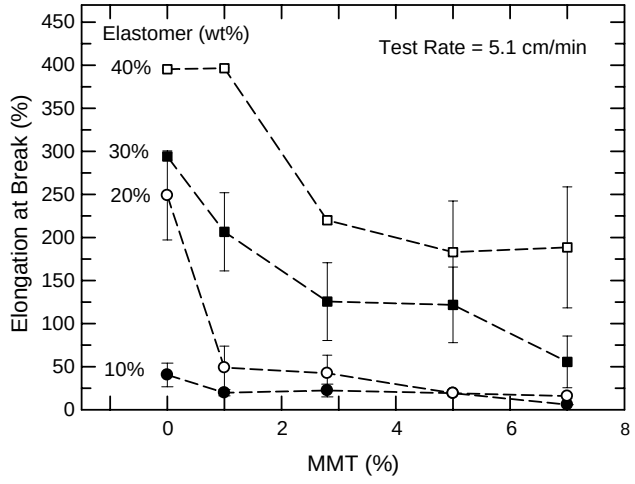

Fig. 19. Effect of MMT and elastomer contents on the elongation at break of PP/elastomer/masterbatch nanocomposites (test speed = 5.1 cm/min).

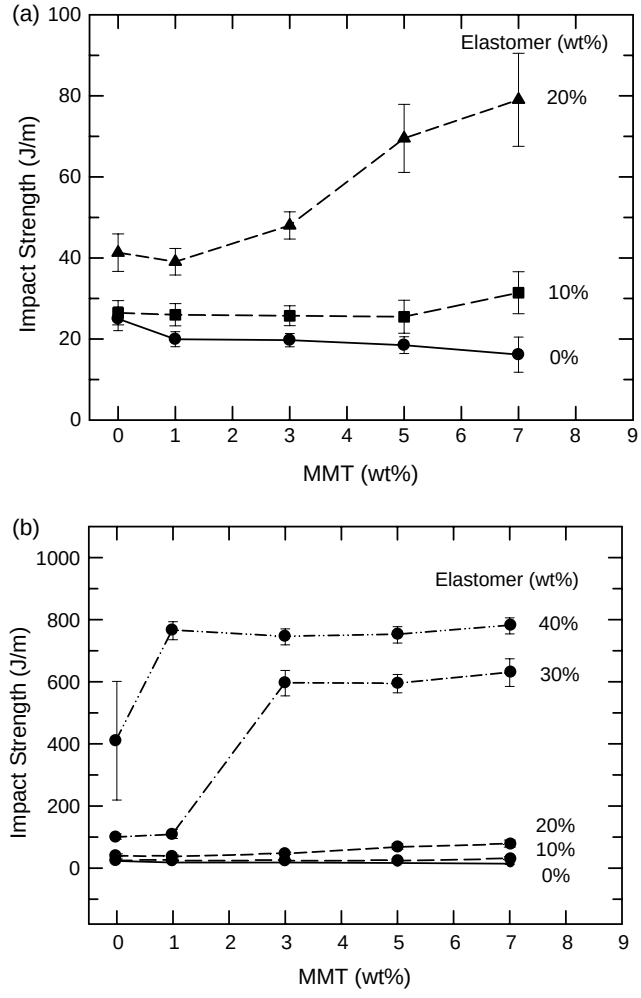

Fig. 20. Effect of MMT and elastomer contents on notched impact strength of PP/elastomer/masterbatch nanocomposites: (a) nanocomposites containing 0, 10 and 20 wt% elastomer and (b) nanocomposites containing higher amounts of elastomer, e.g. 30 and 40 wt%.

nanocomposites with elastomer as shown in Fig. 20(a); these materials are relatively brittle and exhibit complete breakage of the specimen during the impact test as shown in Fig. 21. However, at higher amounts of elastomer, e.g. 30 and 40%, the fracture goes from brittle to ductile as the amount of MMT exceeds a certain value, Fig. 20(b). It is generally expected that an increase in the amount of filler results in a decrease in impact strength of composite materials; however, the trend is opposite for these nanocomposites, i.e. increasing impact strength with increasing MMT content. This unexpected behavior can be explained in terms of morphological changes induced by the dispersion of clay particles, as described in the previous sections. The apparent increase in impact strength for nanocomposites containing higher amounts of elastomer at higher MMT concentrations most likely results from the reduction in the size of the elastomer particle, which may stem from the increase in melt viscosity and the 'barrier' effect the clay particles exert in preventing coalescence of elastomer particles during melt processing.

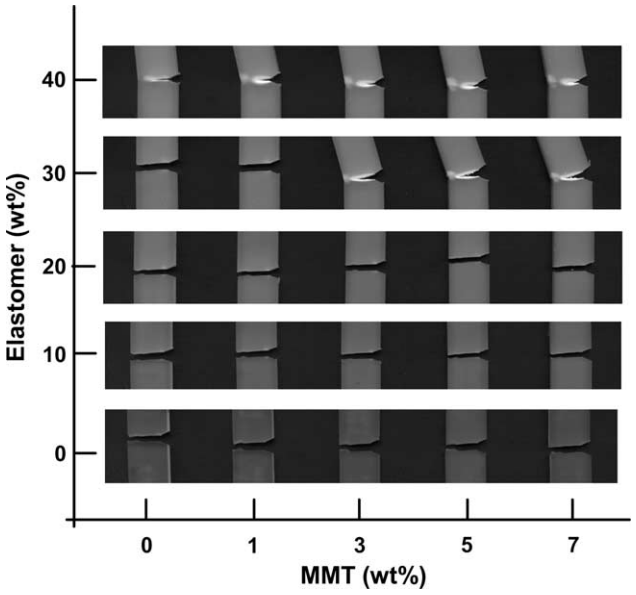

Fig. 21. Photograph of Izod specimens taken after the notched impact test for PP/elastomer/masterbatch nanocomposites containing various amounts of elastomer and MMT.

4. Conclusions

The morphology and mechanical properties of PP/elastomer/organoclay nanocomposites prepared by melt processing have been investigated. Detailed morphological studies and subsequent quantitative particle analyses for the dispersed clay and elastomer phases revealed important features for the morphology of these nanocomposites; firstly, the aspect ratio of the clay particles decreased as the amount of clay in the nanocomposites increased. Secondly, the apparent size of elastomer particles decreased with increasing MMT content, which is most likely due to the increase in melt viscosity and the role of clay particles in preventing coalescence of elastomer particles during processing. The rate of reduction in both particle aspect ratio and elastomer particle size was greater with initial loading of the clay, and, then, both properties decreased slowly with further addition of MMT. The apparent reduction in reinforcement efficiency with increasing MMT shown in modulus data may be attributed to the former morphological changes with varying MMT amounts. The latter observation can explain the apparent toughening behavior of nanocomposites containing higher elastomer contents at higher MMT amounts. There exists a critical elastomer content, particle size and/or interparticle distance beyond which the composites are super-tough.

Acknowledgements

The authors thank General Motors for funding this work and the permission to publish it. The authors would like to thank Dr Douglas Hunter, Mr Ben Knesek, Randy Chapman and Tony Gonzales of Southern Clay Products for technical assistance and providing materials.

References

[1] Okada A, Fukushima Y, Kawasumi M, Inagaki S, Usuk A, Sugiyami S, et al. US Patent No. 4739007; 1988 [assigned to Toyota Motor Co., Japan].
[2] Reichert P, Nitz H, Klinke S, Brandsch R, Thomann R, Mulhaupt R. Macromol Mater Eng 2000;275:8–17.
[3] Vaia RA, Giannelis EP. MRS Bull 2001;26(5):394–401.
[4] Dennis HR, Hunter DL, Chang D, Kim S, White JL, Cho JW, et al. Polymer 2001;42(23):9513–22.
[5] Kawasumi M, Hasegawa N, Kato M, Usuki A, Okada A. Macromolecules 1997;30(20):6333–8.
[6] Hasegawa N, Kawasumi M, Kato M, Usuki A, Okada A. J Appl Polym Sci 1998;67(1):87–92.
[7] LeBaron PC, Wang Z, Pinnavaia TJ. Appl Clay Sci 1999;15(1–2): 11–29.
[8] Garces JM, Moll DJ, Bicerano J, Fibiger R, McLeod DG. Adv Mater 2000;12(23):1835–9.
[9] Hasegawa N, Okamoto H, Kawasumi M, Kato M, Tsukigase A, Usuki A. Macromol Mater Eng 2000;280/281:76–9.
[10] Ishida H, Campbell S, Blackwell J. Chem Mater 2000;12(5): 1260–7.
[11] Liu X, Wu Q. Polymer 2001;42(25):10013–9.
[12] Marchant D, Jayaraman K. Ind Eng Chem Res 2002;41(25): 6402–8.
[13] Garcia-Lopez D, Picazo O, Merino JC, Pastor JM. Eur Polym J 2003; 39(5):945–50.
[14] Hasegawa N, Usuki A. J Appl Polym Sci 2004;93(1):464–70.
[15] Ellis TS, D'Angelo JS. J Appl Polym Sci 2003;90(6):1639–47.
[16] Karger-Kocsis J, editor. Polypropylene; strucuture, blends and composites. Cambridge: Chapman & Hall; 1995.
[17] Collar EP, Areso S, Laguna O, Garcia-Martinez JM. J Polym Mater 1998; 15(3):237–42.
[18] Stamhuis JE. Polym Compos 1988;9(4):280–4.
[19] Garcia-Martinez JM, Laguna O, Areso S, Collar EP. J Polym Sci, Part B: Polym Phys 2002;40(13):1371–82.
[20] Data provided by D.L. Hunter of Southern Clay Products Inc.
[21] Jancar J, Dibenedetto AT. J Mater Sci 1994;29(17):4651–8.
[22] Jang BZ, Uhlmann DR, Vander Sande JB. J Appl Polym Sci 1985;30(6): 2485–504.
[23] Long Y, Shanks RA. J Appl Polym Sci 1996;62(4):639–46.
[24] Premphet-Sirisinha K, Preechachon I. J Appl Polym Sci 2003;89(13): 3557–62.
[25] Ou Y-C, Guo T-T, Fang X-P, Yu Z-Z. J Appl Polym Sci 1999;74(10): 2397–403.
[26] Li Y, Wei G-X, Sue H-J. J Mater Sci 2002;37(12):2447–59.
[27] Tjong SC, Meng YZ. J Polym Sci, Part B: Polym Phys 2003;41(19): 2332–41.
[28] Mehta S, Mirabella FM, Rufener K, Bafna A. J Appl Polym Sci 2004; 92(2):928–36.
[29] Fornes TD, Paul DR. Polymer 2003;44(17):4993–5013.
[30] Yoon PJ, Fornes TD, Paul DR. Polymer 2002;43(25):6727–41.
[31] Chin IJ, Thurn-Albrecht T, Kim HC, Russell TP, Wang J. Polymer 2001; 42(13):5947–52.
[32] Yalcin B, Cakmak M. Polymer 2004;45(19):6623–38.
[33] Jiang W, Liu C-H, Wang Z-G, An L-J, Liang H-J, Jiang B-Z, et al. Polymer 1998;39(14):3285–8.
[34] Liang JZ, Li RKY. J Appl Polym Sci 2000;77(2):409–17.
[35] Galgali G, Ramesh C, Lele A. Macromolecules 2001;34(4):852–8.
[36] Fornes TD, Yoon PJ, Keskkula H, Paul DR. Polymer 2001;42(25): 9929–40.
[37] Solomon MJ, Almusallam AS, Seefeldt KF, Somwangthanaroj A, Varadan P. Macromolecules 2001;34(6):1864–72.
[38] Gu S-y, Ren J, Wang Q-f. J Appl Polym Sci 2004;91(4):2427–34.
[39] Wu S. Polymer 1987;27:335.
[40] Khatua BB, Lee DJ, Kim HY, Kim JK. Macromolecules 2004;37(7): 2454–9.

[41] Nam PH, Maiti P, Okamoto M, Kotaka T, Hasegawa N, Usuki A. Polymer 2001;42(23):9633–40.
[42] Lincoln DM, Vaia RA, Wang Z-G, Hsiao BS. Polymer 2001;42(4):1621–31.
[43] Usuki A, Koiwai A, Kojima Y, Kawasumi M, Okada A, Kurauchi T, et al. J Appl Polym Sci 1995;55(1):119–23.
[44] Wu S. Polymer 1985;26(12):1855–63.
[45] Jiang W, Tjong SC, Li RKY. Polymer 2000;41(9):3479–82.
[46] Jiang W, Yu D, Jiang B. Polymer 2004;45(19):6427–30.
[47] Jiang W, Yu D, An L, Jiang B. J Polym Sci, Part B: Polym Phys 2004; 42(8):1433–40.
[48] Hasegawa N, Okamoto H, Kato M, Usuki A. J Appl Polym Sci 2000; 78(11):1918–22.